Experimental and *ab initio* study of the photofragmentation of DNA and RNA sugars

D. T. Ha,[1,2,*] M. A. Huels,[3] M. Huttula,[4] S. Urpelainen,[4] and E. kukk[1,5]

[1]*Department of Physics and Astronomy, University of Turku, Finland*

[2]*Graduate School of Materials Research, Turku, Finland*

[3]*Department of Nuclear Medicine and Radiobiology, Faculty of Medicine, University of Sherbrooke, Sherbrooke, Quebec, Canada*

[4]*Department of Physics, University of Oulu, Finland*

[5]*Turku University Centre for Materials and Surfaces (MatSurf), Turku, Finland*

(Received 28 June 2011; published 26 September 2011)

The photoelectron-photoion-photoion coincidence method is used to measure the photodissociation of doubly charged D-ribose ($C_5H_{10}O_5$), the RNA sugar molecules, and 2-deoxy-D-ribose ($C_5H_{10}O_4$), the DNA sugar molecules, following normal Auger decay after initial C 1*s* and O 1*s* core ionizations. The fragment identification is facilitated by measuring isotopically labeled D-ribose, such as D-ribose deuterated at C(1), and with ^{13}C at the C(5) position. *Ab initio* quantum chemistry calculations are used to gain further insight into the abundant appearance of the CHO^+ fragment.

DOI: 10.1103/PhysRevA.84.033419 PACS number(s): 33.80.Eh

I. INTRODUCTION

D-ribose is a monosaccharide with the chemical formula of $C_5H_{10}O_5$, whereas 2-deoxy-D-ribose contains one less O atom, as shown in Figs. 1(a) and 1(b). Both monosaccharides can be found in three different conformations: a linear form, a furanose (five-membered ring), and a pyranose (a six-membered ring). In the furanose form, D-ribose is a constituent of RNA, whereas 2-deoxy-D-ribose comprises the backbone of DNA. However, according to the results in the research of Guler *et al*. [1] and others on the reactivity of monosaccharides, free monosaccharides are cyclic molecules and maintain their pyranose forms throughout the evaporation procedure.

DNA and RNA are the carriers of the genetic instructions needed for the development and functioning of all known living organisms, hence understanding the effects of radiation damage on them cannot be overemphasized. Radiation damage on DNA and RNA can lead to serious genetic effects via structural damage causing a single- or double-strand break, or via releasing nucleobases or chemical modification of the nucleobases [2]. Because of their radiobiological relevance, there exists a wide range of research on genetic sugars. Particularly relevant to this study are the works of Ptasinska *et al*. [3] and Vall-llosera *et al*. [4] on valence ionization-fragmentation of 2-deoxy-D-ribose in the gas phase induced by electron and VUV photon interactions, and the works of Fujii *et al*. [5] and Deng *et al*. [6] on soft-x-ray and low-energy ion damage to thin films of DNA components, including genetic sugars, bases, and nucleosides. Both of these latter studies suggested that in DNA and RNA, the monosaccharides are the more fragile moieties in the sugar-phosphate backbone, and underscored the similarities of the damage efficiency of soft x rays and heavy particles.

In this work, we present a very detailed fragmentation study of D-ribose ($C_5H_{10}O_5$), denoted here as DR, and 2-deoxy-D-ribose ($C_5H_{10}O_4$), denoted as DRO, induced by soft x rays using monochromatic synchrotron radiation. The electron-energy-resolved, photoelectron-photoion-photoion coincidence (PEPIPICO) technique [7–11] was used to record the photodissociation fragments of doubly charged DR and DRO in coincidence with the carbon 1*s* photoelectrons, and also of doubly charged DRO in coincidence with the oxygen 1*s* photoelectrons. The dicationic states of the parent molecules were created as the result of initial core ionization by soft-x-ray absorption, followed by normal Auger decay of the core hole. The PEPIPICO measurements were also performed on deuterated D-ribose at C(1), denoted as DRD, and a D-ribose (DRC) where $^{12}C(5)$ is replaced by the ^{13}C isotope [see Figs. 1(c) and 1(d)] in order to reduce the ambiguity of the origins and the identities of ionic fragment pairs. The 2-deoxy-D-ribose molecule also serves the same purpose, since it deviates from D-ribose only by one missing O atom at C(2). All samples in this work were measured as free molecules in the gas phase by thermal evaporation. Although examining the isolated sugar molecule does not give us a direct picture of the fracturing of full DNA and RNA itself, the present research provides a fundamental aspect of the fragmentation mechanisms and gives important insight into how DNA and RNA damage takes place at the nanoscopic molecular level of the individual DNA and RNA components.

II. EXPERIMENTAL METHODS

The apparatus used for the present PEPIPICO experiments is described thoroughly in Refs. [12–14]. A brief summary of the hardware and the experimental variables are presented here. The apparatus consists of a homemade Wiley-McLaren-type ion time-of-flight (TOF) detector with a 400-mm-long drift tube and a modified Scienta SES-100 electron energy analyzer [15]. The original CCD camera of the electron spectrometer was replaced by a resistive anode detector. The TOF spectrometer is equipped with a 70-mm Hamamatsu micro-channel plate (MCP) detector. The ion-detection electronics is based on a 1-GHz waveform digitizer card (Signatec PDA 1000).

The PEPIPICO measurements were performed in pulsed-field mode, where the detection of electrons by the electron

*DangTrinh.Ha@utu.fi

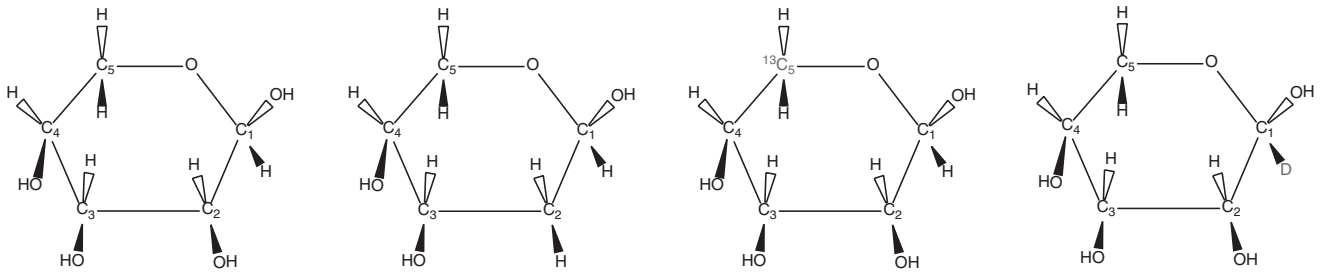

FIG. 1. (a) D-ribose, (b) 2-deoxy-D-ribose, (c) D-ribose with C(5) is isotopically labeled, and (d) deuterated D-ribose.

analyzer triggers the clock for the TOF measurement of the ions. The recorded signals of an electron and the ions related to the same events belong to so-called true coincidences. In contrast, false coincidences are such events where the ion TOF spectrometer detects one or more fragments from a different molecule than the one emitting the detected electron. The false/true coincidence ratio was kept at a minimum by using low count rates of about 10 e/s. In addition, a pulse generator was used during the PEPIPICO measurements to provide noncoincident extraction pulses at a constant frequency. The signals of ion-ion coincidences were initially triggered in two different ways—by electrons and by pulse generator—and were collected simultaneously. The average number of ions per electron trigger and the number of ions per artificial trigger (including detector noise counts) was, respectively, 0.8 and 0.4 in the case of C 1*s* core ionization in DR, 0.9 and 0.4 in DRC and DRD, and 1.1 and 0.6 in DRO C 1*s*, but 1.0 and 0.5 for O 1*s* core ionization in DRO. The acquired data were then analyzed with the help of custom-made IGOR PRO software-based data-analysis macros [16] to retrieve two-dimensional (2D) PEPIPICO maps of real coincidence patterns.

The D-ribose and 2-deoxy-D-ribose samples were purchased from Sigma-Aldrich with purity greater than 99%, while the ^{13}C and deuterium-labeled D-ribose were purchased from Cambridge Isotopes, with isotopic purities of 98%. During the measurements, the samples were evaporated into the sample area using an effusion cell with an integrated cooling shroud (MBE Komponenten NTEZ40 oven) at temperatures ranging from 80 to 92 °C. The experiments were performed at the undulator-based soft-x-ray beamline I411 at the MAX-II synchrotron radiation storage ring (Lund University, Sweden) [17]. The undulator radiation was monochromatized by a Zeiss SX-700 plane-grating monochromator. The photon energy used for the PEPIPICO measurements was $h\upsilon = 330$ eV to retrieve C 1*s* photoelectrons, and $h\upsilon = 578$ eV in the case of O 1*s* photoelectrons. The electron kinetic-energy window was set to range from 32 to 44 eV, with the photon bandwidth being 400 meV. The entrance slit of the electron spectrometer was 1.6 mm and the pass energy was 100 eV, which corresponds to the energy resolution of 750 meV in photoelectron kinetic energy. During the experiments, the chamber pressure was typically in the 10^{-7} mbar range. The x-ray photoelectron spectroscopy (XPS) measurements were performed with the same setting parameters as in the PEPIPICO measurements.

III. RESULTS AND DISCUSSION

A. Photoelectron spectra

C 1*s* binding energies of the sugar molecules vary on the basis of the chemical environments of carbon atoms in the molecules. The C 1*s* photoelectron spectra in Fig. 2 show the C 1*s* binding energies with different chemical shifts in DR and DRO molecules. The peaks in the spectra were decomposed by the curve-fitting package SPANCF [16], and identified based on the electronegativity of the chemical environments of the carbon atoms and also on the molecular orbital energies (calculated by using the theory described in Sec. III D) of the molecules. The peak at the binding energy of 292.3 eV in the spectrum of DR is assigned to carbons at the C(2,3,4,5) sites, and the high binding-energy shoulder at 293.7 eV to the C(1) carbon. In comparison with the spectrum of the DR molecule, C 1*s* binding energy of the C(2) carbon in the DRO molecule is shifted to $E_b = 290.9$ eV, since the oxygen bonded to it is replaced by hydrogen. Consequently, the highest peak at $E_b = 292.2$ eV in the spectrum of DRO is narrower than the one of DR, and therefore the peak at the binding energy of 293.7 eV [corresponding to C 1*s* binding energy of carbon C(1)] in the spectrum of DRO is singly resolved. With the spectra unambiguously resolved and assigned to solely C 1*s* binding energies of the carbon sites in DR and DRO molecules, one can rely on the fact that the sample molecules maintained their pyranose forms and did not dissociate at the measurement temperature before irradiation.

B. Overview

After creating a 1*s* core hole in one of the C atoms (with photon energy of $h\upsilon = 330$ eV) in the target molecules, an Auger electron is emitted via a relaxation process resulting in doubly charged molecules, which have a high tendency to degrade into smaller fragments via various multibody fragmentation mechanisms [18]. In the present experiment, positive ionic fragments were detected, and their mass-to-charge ratios were determined by their flight time in the TOF tube. In a typical data presentation, the acquired flight times of faster ions are plotted along the *x* axis and the flight times of the slower ions along the *y* axis to form a 2D TOF correlation map, i.e., a PEPIPICO map, with patterns corresponding to the various momentum-correlated cation pairs detected. Depending on kinematics and the orientational distribution of the dissociating molecules,

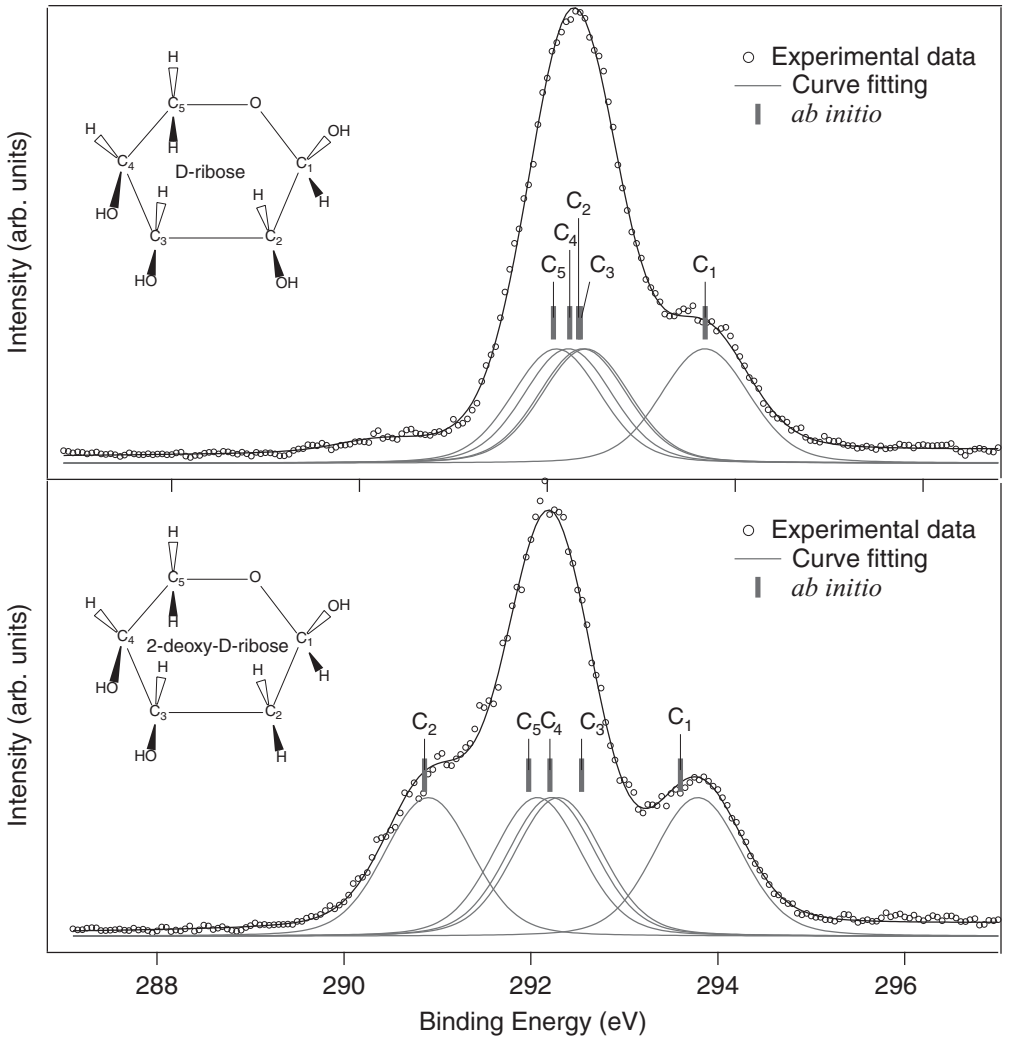

FIG. 2. C 1*s* photoelectron spectra of D-ribose (upper) and 2-deoxy-D-ribose (lower) with curve fitting. The vertical bars correspond to theoretical assignments of the C 1*s* binding energies of carbons in different chemical environments in the sugar molecules.

the patterns can be seen with various widths and tilted angles. Blurring of the patterns occurs due to the presence of neutral ("dark") fragments, reducing the momentum correlation of the ions. The patterns close to the diagonal of equal flight times (ascribed to ions with the same mass-to-charge ratio) are incomplete, resulting from deadtime effects that prevented detecting ions arriving less than 30 ns apart. The ion TOFs can be converted to mass-to-charge (m/z) ratios by using the formula $m/z = (T_{\mathrm{TOF}} - T_0)^2/C^2$, where the calibration parameters are $T_0 = 198.0$ and $C = 1066.0$ for DR, $T_0 = 208.7$ and $C = 1063.1$ for DRO, $T_0 = 214.4$ and $C = 1063.6$ for DRC, and $T_0 = 201.6$ and $C = 1064.9$ for DRD. The PEPIPICO map of true coincidences based on the measured data of the D-ribose molecule is shown in Fig. 3. Fragment masses in the figure labels and in the following text are given in atomic mass units. With the simple chemical composition of these molecules consisting only of C, H, and O atoms, chemical fragment identification based on their mass-to-charge ratio is quite straightforward. In contrast, determining the site origin of the fragment in the parent ring molecule, and, consequently, attempting to describe the fragmentation processes is more challenging.

Tables I and II list all coincident cation pairs corresponding to the strongest patterns detected in the C 1*s* photoionization fragmentation measurements on D-ribose and 2-deoxy-D-ribose (Table I), and ^{13}C and deuterium-labeled D-ribose (Table II). Let us first consider the yields of individual fragment ions regardless of the coincident pairs that they form: the most intense fragments observed from PEPIPICO measurements of DR (left half of the table) are CH_2^+ ($m/z = 14$), CH_3^+ (15), OH_2^+ (18), OH_3^+ (19), $C_2H_2^+$(26), $C_2H_3^+$(27), CHO^+ (29), CH_3O^+ (31), $C_2H_2O^+$ (42), and $C_2H_3O^+$ (43). These cover about 76% of the total ion yield after the C 1*s* ionization. The CHO^+ fragment, or aldehyde (or formyl) cation, has the strongest intensity (32%) compared to any other m/z number in these dissociation processes, and it is seen in pairs with every fragment, including another $m/z = 29$, listed above. This is easily understood, as the fragment can originate, without any rearrangement, from four (in DR) or three (in DRO) different parent ring locations [see Figs. 1(a) and 1(b)]. However, at the

TABLE I. The coincident cation pairs detected in the PEPIPICO measurements of DR (left half of the table) and DRO (right half of the table) in coincidence from C 1*s* photoionization at 330 eV photon energy.

	DR				DRO		
Fragment 1	M_1	M_2	Fragment 2	Fragment 1	M_1	M_2	Fragment 2
CH_2^+	14	29	CHO^+	CH_2^+	14	29	CHO^+
CH_3^+	15	15	CH_3^+	CH_3^+	15	15	CH_3^+
				CH_3^+	15	18	OH_2^+
				CH_3^+	15	19	OH_3^+
CH_3^+	15	29	CHO^+	CH_3^+	15	29	CHO^+
				CH_3^+	15	27	$C_2H_3^+$
CH_3^+	15	31	CH_3O^+	CH_3^+	15	31	CH_3O^+
				CH_3^+	15	43	$C_2H_3O^+$
OH_2^+	18	29	CHO^+	OH_2^+	18	29	CHO^+
OH_3^+	19	29	CHO^+	OH_3^+	19	29	CHO^+
				$C_2H_3^+$	27	27	$C_2H_3^+$
$C_2H_2^+$	26	29	CHO^+	$C_2H_2^+$	26	29	CHO^+
$C_2H_3^+$	27	29	CHO^+	$C_2H_3^+$	27	29	CHO^+
				$C_2H_3^+$	27	31	CH_3O^+
				$C_2H_3^+$	27	42	CH_2O^+
				$C_2H_3^+$	27	43	CH_3O^+
$C_2H_4^+$	28	29	CHO^+	$C_2H_4^+$	28	29	CHO^+
CHO^+	29	29	CHO^+	CHO^+	29	29	CHO^+
CHO^+	29	31	CH_3O^+	CHO^+	29	31	CH_3O^+
				CHO^+	29	39	$C_3H_3^+$
CHO^+	29	42	$C_2H_2O^+$	CHO^+	29	42	$C_2H_2O^+$
CHO^+	29	43	$C_2H_3O^+$	CHO^+	29	43	$C_2H_3O^+$
CH_3O^+	31	42	$C_2H_2O^+$	CH_3O^+	31	42	$C_2H_2O^+$
CH_3O^+	31	43	$C_2H_3O^+$	CH_3O^+	31	43	$C_2H_3O^+$
				$C_2H_3O^+$	43	43	$C_2H_3O^+$

same time, the absence (or weak traces) of fragment CH_2O^+ (30) is noteworthy considering that these are most likely the moieties that are the precursors of the CHO^+ fragments. We will return to this question in connection with the *ab initio* calculations.

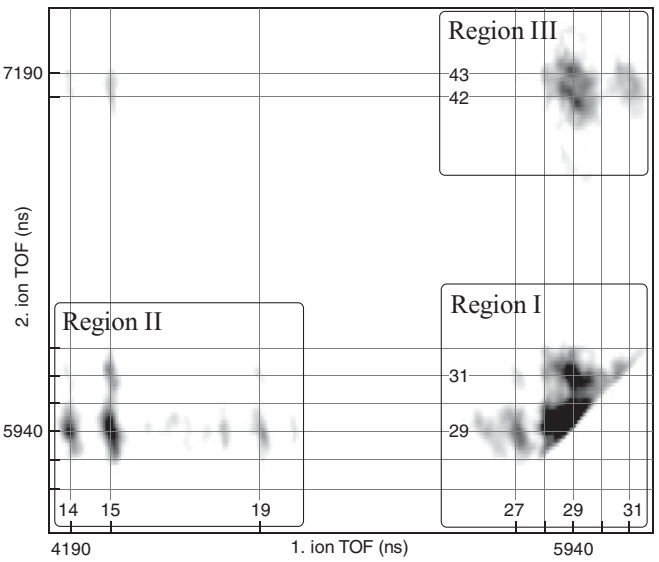

FIG. 3. PEPIPICO map of D-ribose in coincidence with C 1*s* photoelectrons. Grid lines inside the map are labeled by mass numbers in atomic mass units.

C. Fragmentation processes

In this section, we will follow the contents of Tables I and II and examine the dissociation processes by comparing the patterns on the PEPIPICO maps shown later in this text. The analysis is divided into three main regions (I, II, and III) as shown on the map in Fig. 3.

First, we inspect region I that contains the most intense patterns. The region is shown in detail in Fig. 4, using contour plots to make the shifts of the patterns from sample to sample easier to follow.

1. The $C_2H_3^+$ and CHO^+ channel

Let us start from the pattern (27,29) in DR [Fig. 4(a)], which is not the strongest but has a well-defined, momentum-correlated shape. Its chemical assignment is clear, i.e., $C_2H_3^+$, CHO^+, if we discard the very unlikely possibility of fragments like $C_2H_5^+$. One notices that the $^{13}C(5)$ substitution almost eliminates the (27,29) pattern [Fig. 4(c)], while giving strength to the (28,29) pattern. This suggests that the coincident ion $C_2H_3^+$ in these events includes isotope ^{13}C and, therefore, its molecular origin is almost exclusively the C(5) site in the molecule. Nevertheless, the small remaining amount of pattern (27,29) on the DRC map [see Fig. 4(c)] means that a small amount of the ion $C_2H_3^+$ originates elsewhere in the molecule, in which case hydrogen migration from a neighboring group is required during the dissociation process.

TABLE II. The coincident cation pairs detected in the PEPIPICO measurements of DRC (right half of the table) and DRD (left half of the table) in coincidence from the C 1*s* photoionization at 330 eV photon energy. The underlined mass numbers are increased (+1 amu) due to the isotopic labeling.

	DRD				DRC		
Fragment 1	M_1	M_2	Fragment 2	Fragment 1	M_1	M_2	Fragment 2
CH_3^+	15	15	CH_3^+	CH_3^+	15	15	CH_3^+
CH_2^+	14	29	CHO^+	CH_2^+	14	29	CHO^+
CH_3^+	15	29	CHO^+	CH_3^+	15	29	CHO^+
CH_3^+	15	<u>30</u>	CDO^+	CH_3^+	15	<u>30</u>	$^{13}CHO^+$
CDH_2^+	<u>16</u>	29	CHO^+	$^{13}CH_3^+$	<u>16</u>	29	CHO^+
CH_3^+	15	31	CH_3O^+	CH_3^+	15	31	CH_3O^+
OH_2^+	18	29	CHO^+	OH_2^+	18	29	CHO^+
OH_3^+	19	29	CHO^+	OH_3^+	19	29	CHO^+
$C_2H_2^+$	26	29	CHO^+	$C_2H_2^+$	26	29	CHO^+
$C_2H_3^+$	27	29	CHO^+	$C_2H_3^+$	27	29	CHO^+
				$^{13}CCH_3^+$	<u>28</u>	29	CHO^+
$C_2H_4^+$	28	29	CHO^+	$C_2H_4^+$	28	29	CHO^+
CHO^+	29	29	CHO^+	CHO^+	29	29	CHO^+
CHO^+	29	<u>30</u>	CDO^+	CHO^+	29	<u>30</u>	$^{13}CHO^+$
CHO^+	29	31	CH_3O^+	CHO^+	29	31	CH_3O^+
CHO^+	29	<u>32</u>	CDH_2O^+	CHO^+	29	<u>32</u>	$^{13}CH_3O^+$
CHO^+	29	42	$C_2H_2O^+$	CHO^+	29	42	$C_2H_2O^+$
CHO^+	29	43	$C_2H_3O^+$	CHO^+	29	43	$C_2H_3O^+$
				CHO^+	29	<u>44</u>	$^{13}CCH_3O^+$
CDO^+	<u>30</u>	31	CH_3O^+	$^{13}CHO^+$	<u>30</u>	31	CH_3O^+
CDO^+	<u>30</u>	42	$C_2H_2O^+$	$^{13}CHO^+$	<u>30</u>	42	$C_2H_2O^+$
CH_3O^+	31	42	$C_2H_2O^+$	CH_3O^+	31	42	$C_2H_2O^+$
CH_3O^+	31	<u>43</u>	$C_2DH_2O^+$	CH_3O^+	31	<u>43</u>	$^{13}CCH_2O^+$
CH_3O^+	31	43	$C_2H_3O^+$	CH_3O^+	31	43	$C_2H_3O^+$

Considering the geometry of the parent molecule, it seems that fragment $C_2H_3^+$ formed at C(5) naturally also involves C(4) [see Figs. 5(a) and 5(b)]. Returning to Fig. 4, we further notice that the pattern assigned to the ion pair (27,29) on the DRO map (b) has higher intensity than the corresponding patterns on any other maps, which is obviously due to the lack of the hydroxyl group at C(2). In other words, due to the additional HCH group at C(2) in 2-deoxy-D-ribose, the $C_2H_3^+$ fragment can be created by severing either the C(1)-C(2) and C(3)-C(4), or the C(2)-C(3) and C(1)-O bonds.

The intensities of the patterns (27,29) on the DR and DRD map [Figs. 4(a) and 4(d)] have approximately equal intensities. However, one can see on the DRD map that there is some intensity transfer from the (27,29) to (27,30) region, the latter of which is completely void of intensity on the DR map. Thus, a minor fraction of the heavier fragment in this pair, CHO^+, contains the C(1)-H moiety, which was deuterated in the DRD sample. Figure 5 combines the information from all four samples by presenting the most likely fragmentation mechanisms yielding the $C_2H_3^+$, CHO^+ pair in DR.

In brief, we have seen that the $C_2H_3^+$ (27) cations can be produced most likely from HCH-HCOH moieties [containing the C(5) site that binds to a phosphate in DNA and RNA, and also the C(3) site in 2-deoxy-D-ribose that binds to a phosphate in DNA] by ejecting a whole hydroxyl group. The CHO^+ (29)

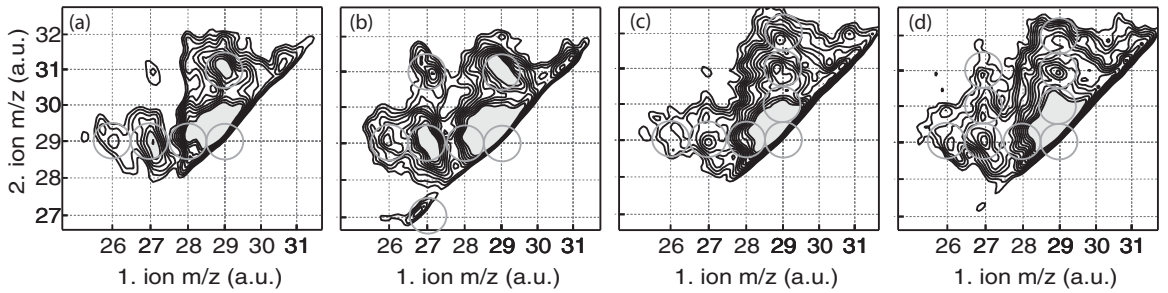

FIG. 4. The PEPIPICO maps (coincident with C 1*s* electron) in region I of (a) DR, (b) DRO, (c) DRC, and (d) DRD are presented in contour in order to better visualize the shifting of patterns. Note that the axes are in atomic mass units instead of TOF. The fragment pairs circled in light gray color are discussed in the text.

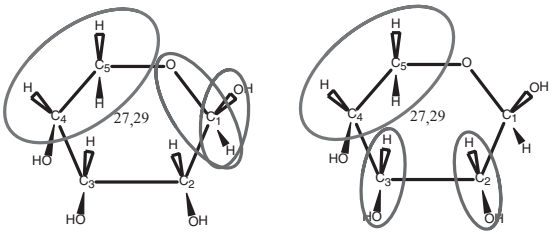

FIG. 5. Possible dissociation channels producing the ion pair $C_2H_3^+$ and CHO^+ (27,29) from D-ribose.

cations can originate from HCOH moieties, which will be discussed in greater detail later in this work.

2. The CHO^+ and CH_3O^+ channel

Now we examine the pattern (29,31) on the DR map shown in Fig. 4(a), which is ascribed to the ion pair CHO^+ and CH_3O^+. On the DRC and DRD map in Figs. 4(c) and 4(d), one can notice that the substitution of $^{13}C(5)$ in DRC and deuterium at C(1) in DRD transfer some intensity from pattern (29,31) to pattern (29,32). That is to say, the CH_3O^+ fragment can come from both sites C(5) or C(1). The intensity differences of the shifted patterns (29,32) on both DRC and DRD maps are not significant, though the C(5) site seems to give a slightly stronger signal than the C(1). Nearby to this ion pair, the shifted pattern (30,31) on the DRC and DRD maps in Figs. 4(c) and 4(d) suggests that C(1) and C(5) can also be part of the departing CHO^+s. The remaining unshifted intensity of the pattern (29,31) on both DRC and DRD maps involves other origins of the fragments, which can be explained by several possible fragmentation channels. However, further insight into the principal dissociation dynamics can be obtained from the PEPIPICO maps using the slopes of the patterns that exhibit momentum correlation, as these reveal the step-by-step division of the molecular mass in a multistage dissociation process. In general, slope $k \approx -1$ (the width of the pattern along the TOF axis of the heavier fragment, divided by the width along the lighter fragment's TOF axis) of the rather broad pattern (29,31) on the DR map suggests that the ion pair CHO^+ and CH_3O^+ is ejected in a two-step (delayed charge separation) process in which a low-kinetic-energy neutral fragment is released prior to charge separation of a dication fragment. In the next charge separation phase, the dicationic fragment $C_2H_4O_2^{++}$ dissociates into CHO^+ and CH_3O^+ in such way

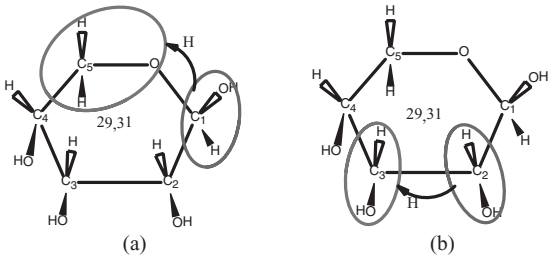

FIG. 6. Fragmentation schemes producing the ion pair CHO^+ and CH_3O^+ (29,31) from D-ribose; the doubly charged parent molecule releases a neutral fragment, which is followed by charge separation of the remaining dicationic fragment $C_2H_4O_2^{++}$.

that the moiety creating cation CHO^+ donates a hydrogen atom to the adjacent part forming the CH_3O^+ [see examples in Figs. 6(a) and 6(b)]. These fragments do not dissociate further.

In short, the HCOH group serves as a precursor moiety creating aldehyde (29) cations by dissipating a hydrogen from the hydroxyl group, or capturing a hydrogen atom from a neighboring group during the fragmentation process to yield CH_3O^+ (31).

3. The $C_2H_3^+$ and CH_3O^+ channel

When comparing the areas at coordinates (27,31) amu on the maps in Figs. 4(a)–4(d), one notices that a weak pattern (27,31) is discernible only on the DRO map. The appearance of this ion pair is probably linked to the existence of two HCH sites in 2-deoxy-D-ribose, namely, at C(5) and C(2). The fragmentation channels most likely creating the ion pair $C_2H_3^+$ and CH_3O^+ are those where the $H_2C(5)$-O group captures the hydrogen from the C(1) site to form the CH_3O^+ cation, and the $C_2H_3^+$ cation is formed from the C(2) site plus a CH group from either adjacent HCOH moiety.

4. The $C_2H_2^+$ and CHO^+ channel

A weak pattern at (26,29) in Figs. 4(a)–4(d) is ascribed to the $C_2H_2^+$ and CHO^+ pair. Forming the $C_2H_2^+$ cation requires two adjacent C carbon sites dissipating two hydroxyl groups from a HCOH-HCOH moiety or a hydroxyl group plus a hydrogen atom from a HCOH-HCH moiety. Such rearrangements are obviously energetically unfavorable, which explains the low intensity of the pattern.

5. The CHO^+ and CHO^+ channel

Before leaving region I, we discuss the most intense pattern (29,29) on the DR map [see Fig. 4(a)]. As CHO^+ is the most intense individual fragment and can originate from several different ring locations, also simultaneously in the same event, it is expected to form a strong coincidence pattern with itself. First, a comparison of the intensity at coordinates (29,30) on all maps in Figs. 4(a)–4(d) shows that the ion pair (29,30) is seen only on the PEPIPICO maps of DRC (c) and DRD (d); hence, some of the CHO^+ fragments can contain C(1) and C(5). Second, the intense remaining pattern (29,29) on the DRC and DRD maps shows that CHO^+ can also originate elsewhere from ring locations other than C(1) and C(5). Besides, the C(5)-O ring bond is weakest in the molecule due to internal hydrogen bonding, therefore, the forming of CHO^+ at C(5) is less likely in either the normal or the ^{13}C labeled D-ribose. Thus, all the remaining sites that could yield CHO+ are sites with HCOH moiety. Accordingly, the CDO^+ yield in deuterated D-ribose is only a fraction of the (29,29) signal, which is due to the fact that the C(1) site most likely contributes stoicometrically to the total CHO^+ yield, and all the other carbon sites together [i.e., the C(2), C(3), and C(4)] give the signal at (29,29) in deuterated D-ribose. Thus, the bottom line is that the CHO^+ and CHO^+ pair can be formed with greater likelihood at the C(1), C(3), and C(4) carbons in 2-deoxy-D-ribose, and also at the C(2) carbons in D-ribose. Based on the research of Guerra *et al.* [19], one can expect a hydrogen to depart from O-H more likely than C-H in the production of ion CHO^+ from an HCOH moiety. The hydrogen-ejection competition between C-H and

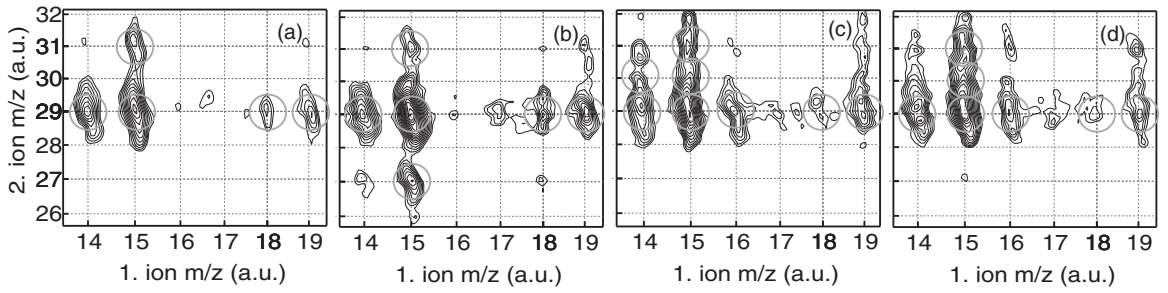

FIG. 7. Regions II of the C 1*s* PEPIPICO maps for (a) DR, (b) DRO, (c) DRC, and (d) DRD. The fragment pairs circled in light gray color are discussed in the text.

O-H in $HCOH^+$ moieties will also be discussed further in Sec. III D.

6. Coincidences with light fragments

Now we proceed to inspect the patterns in region II of the PEPIPICO maps presented in detail in Fig. 7. The DR, DRC, and DRD map in Figs. 7(a), 7(c), and 7(d) have no trace of ion pair CH_3^+ and $C_2H_3^+$, but on the DRO map [see Fig. 7(b)], one can easily distinguish pattern (15,27) ascribed to the ion pair CH_3^+ and $C_2H_3^+$. This suggests that both CH_3^+ and $C_2H_3^+$ have to involve an HCH group in the same dissociation event, which is possible only in DRO, because there are two distinct HCH groups in 2-deoxy-D-ribose. The CH_3^+ fragment is probably formed in such a way that a hydrogen migrates from the C(4) site to join the departing CH_2^+ fragment from C(5). In the same process, $C_2H_3^+$ is built up at the other site of the molecule at C(2) by the local CH_2 and also a CH group from either of the neighbors, as shown in Fig. 8(a). The mass pair (15,27) can of course also be formed in such a way that CH_3^+ arises from the C(2) surroundings, and $C_2H_3^+$ from C(5) site together with C(4) site, as illustrated in Fig. 8(b).

The pattern (14,29) ascribed to ion pair CH_2^+ and CHO^+ can be seen on all maps in Figs. 7(a)–7(d). The CH_2^+ cation can originate at least from an HCH group. However, the strong pattern (14,29) and very light pattern (shifted) (14,30) on the map of the ^{13}C substituted D-ribose in Fig. 7(c) implies that the forming of CH_2^+ cation does not necessarily require an HCH moiety. For this reason, the CH_2^+ cation can also originate from an HCOH group, in which case the HCOH moiety must eject a whole hydroxyl group, and either recapture the hydrogen atom from the eliminated hydroxyl group or capture a hydrogen atom from a neighboring group.

The pattern (15,29) on the DR map in Fig. 7(a) is assigned to ion pair CH_3^+ and CHO^+. The steep slope $k \approx -8.1$ of the pattern (15,29) suggests that the fragmentation begins by charge separation: $DR^{++} \rightarrow CHO^+$ and $C_4H_9O_4^+$, and then continues by secondary dissociation where the heavier cation $C_4H_9O_4^+$ is separated into smaller fragments, $C_3H_6O_4$ and CH_3^+. The total kinetic-energy release of the dissociation is 1.4 ± 0.6 eV, as determined on the assumption that the kinetic-energy release in the secondary process is negligible and thus the momentum correlation in the charge-separation phase is preserved.

On the DRC map in Fig. 7(c), only a small intensity transfer occurs from (15,29) to (15,30), which indicates that the cation CHO^+ can involve the C(5) site. In that case, the fragment CH_3^+ has to originate from other ring locations which, however, have no HCH groups. This notion is also supported by a small intensity transfer from pattern (15,29) to (16,29) on the DRD map [Fig. 7(d)], i.e., the formation of a CH_2D^+, CHO^+ pair. The shifting on the DRD map implies that CH_3^+ can involve the C(1) site and, hence, not only an HCH group at C(5) in D-ribose. Therefore, the formation of CH_3^+ at sites other than C(5) in D-ribose requires the loss of a hydroxyl group and the capture of two hydrogens from adjacent sites within the molecule during the dissociation process. On the contrary, the corresponding shift of (15,29) to (16,29) on the DRC map is an obvious proof of CH_3^+ originating from C(5), because the pair (16,29) is not observed on the DR map.

Perhaps the most eye-catching patterns in Figs. 7(a)–7(d) are the pairs (18-19,29) which can be found as dissociation products in all the samples (see also Tables I and II). The pattern (18,29) is very weak, but the other one ascribed to the ion pair OH_3^+ and CHO^+ is stronger. According to the proton impact study on 2-deoxy-D-ribose by Alvarado *et al.* [20], the majority of OH_3^+s is ejected from the molecule and is not formed from residual gas. Cation OH_3^+ is seen together with heavier ions than CHO^+ in the same study. However, in the present work, OH_3^+ is seen coupled only with ion CHO^+. Clearly, the formation of OH_3^+ in the present cases requires the capture of at least two H atoms by a departing OH^+ from within the molecule during the dissociation process, i.e., concerted bond and atom rearrangements. This is often observed during electron-impact (valence) ionization and dissociation of organic molecules in mass spectrometry, where the singly ionized parent molecule has a long period of time for such intramolecular chemical reactions. In that sense, it is interesting that such a fragment can be formed here in the presumably faster dissociation of the initial dication formed by the core-ionization–Auger-decay process.

In conclusion, the HCH group is an essential contributor in producing CH_3^+ (15) and $C_2H_3^+$ (27), and both cations

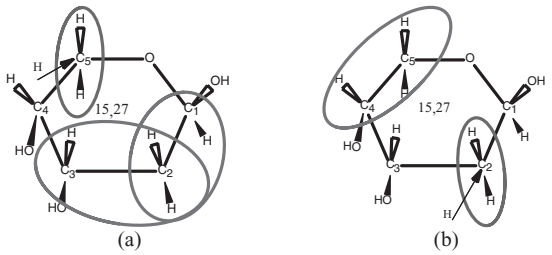

FIG. 8. Three possible dissociation channels producing the ion pair CH_3^+ and $C_2H_3^+$ (15,27) from the 2-deoxy-D-ribose sample.

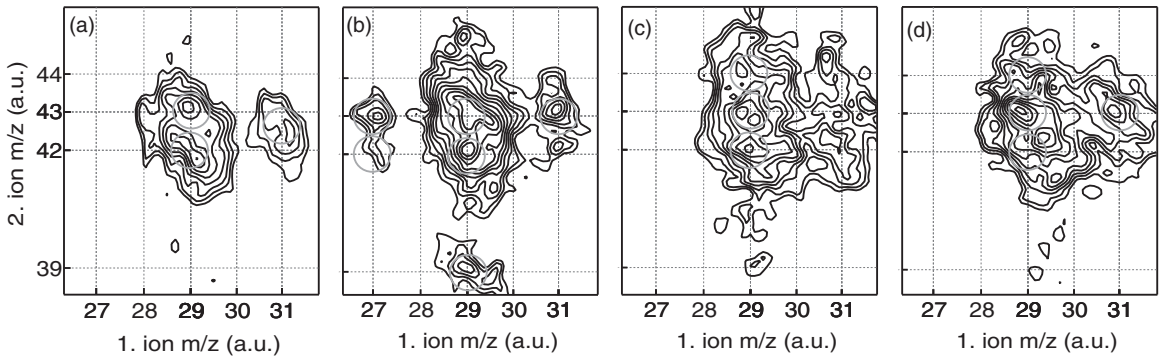

FIG. 9. Regions III of the C 1*s* PEPIPICO maps for (a) DR, (b) DRO, (c) DRC, and (d) DRD. The fragment pairs circled in light gray color are discussed in the text.

can be produced in the same dissociation process only from 2-deoxy-D-ribose. The abundant appearance of the cations can be seen in Table I, where many listed ion pairs of DRO contain CH_3^+ (15) and $C_2H_3^+$ (27) cations. The individual fragments CH_3^+ and $C_2H_3^+$ can also be formed with less probability elsewhere in the molecule, requiring, however, much more complex bond cleavages and rearrangements than the straightforward concerted dissociation case here, where a leaving CH_2^+ (or $C_2H_2^+$) captures a hydrogen atom from the parent molecule. Moreover, inspection of the pattern (14,29) reveals that the CH_2^+ (14) cations most likely originate from the HCH groups. Other moieties, such as HCOH, can also produce the CH_2^+ cation, but with less likelihood. A notable amount of $CH_{2-3}O^+$ (18-19) cations is also produced (in pair with the cation CHO^+).

7. Coincidences with the heaviest fragments

Let us now proceed to region III to examine the rest of the ion pairs. On the DR map in Fig. 9(a), there are two clear patterns at (29,42) and (29,43) that are assigned to the ion pairs (CHO^+, $C_2H_2O^+$) and (CHO^+, $C_2H_3O^+$), respectively. To the right of the patterns is an area considered to contain patterns (31,42) and (31,43), which are ascribed to ion pairs (CH_3O^+, $C_2H_2O^+$) and (CH_3O^+, $C_2H_3O^+$), respectively.

Isotopic labeling of the D-ribose sample results in blurred PEPIPICO maps in this region [see Figs. 9(c) and 9(d)]. In fact, the entire region exhibits a trend to shift the patterns upward for DRD and DRC as compared to DR, which means that the heavier fragments $C_2H_2O^+$ and $C_2H_3O^+$ very likely contain C(1) or C(5). The PEPIPICO map of DRD is diffuse due to the splitting of the patterns of DR into two or more components in DRD, indicating that the eventual localization of deuterium to a certain fragment is not fully determined. The DRC map shows additional intensity both toward increasing the mass of the lighter and the heavier fragment, with possible localization of C(5) in either of the fragments.

The slope $k \approx -1.4$ of the pattern (29,42) (and the pattern 29,43) is consistent with the four-body dissociation mechanism (Ref. [21]), where the ejection of a neutral fragment $H_3OC(3)$-$C(2)OH_2$ is followed by deferred charge separation [$C_3H_5O_3^{++} \rightarrow C_2H_{(2\,or\,3)}O^+$ (42 or 43) and $CH_{(3\,or\,2)}O_2^+$] after which the cation $CH_{(3\,or\,2)}O_2^+$ emits a neutral fragment $H_{(2\,or\,1)}O$ to become CHO^+ (29). Otherwise, supposing a three-body process, where the ion pair was ejected in charge separation followed by secondary dissociation, the slope would be $k \approx -3.7$. The kinetic-energy release in the deferred charge-separation phase [eventually creating the ion pair (29,42)] is 1.4 ± 0.5 eV, as determined assuming that the kinetic-energy release in the secondary process (after the deferred charge-separation phase) is negligible and the momentum correlation in the deferred charge phase is preserved.

A comparison of the intensity at coordinates (31,42-43) on the PEPIPICO map of DR (a) and DRD (d) shows that the pattern (31,42) is almost completely shifted to (31,43) on the map of DRD due to the substitution of deuterium at the C(1) site. Hence, the $C_2H_2O^+$ cation must contain the C(1) site and, naturally, also the C(2) site. The formation of the $C_2H_2O^+$ cation within the above-mentioned conditions requires an HCOH-HCOH moiety to dissipate a hydroxyl group from the other HCOH side and a hydrogen atom from another HCOH side.

The intensity of pattern (31,42) on the map of DRO [Fig. 9(b)] is almost completely shifted to the adjacent pattern (31,43), which is considered to be the consequence of an additional HCH group in 2-deoxy-D-ribose. That is to say, the HCH group is an essential contributor in forming the $C_2H_3O^+$ cation. In addition to the intensity transfer from the pattern (31,42) to the pattern (31,43), there are also unique patterns at (27,43) [and a very weak one at (27,42)] and (29,39), observed only on the DRO map. The first ion pair is consistent with the $C_2H_3^+$ fragment forming around C(2) or C(5) carbons (i.e., HCH groups) in DRO; in other words, the formation of $C_2H_3^+$, $C_2H_3O^+$ (27, 43) ion pairs [and very few $C_2H_3^+$, $C_2H_2O^+$ (27, 42)]. This process is hindered in DR, where an extra OH group replaces one of the two H attached to C(2) in DRO, and thus prevents the formation of both $C_2H_3^+$ and $C_2H_3O^+$ in the same dissociation process. One recalls here another unique pattern of DRO, i.e., (15,27), which also agrees well with the above description, and favors the bond breakage pattern of Fig. 8(a). The (29,39) pattern is ascribed to the ion pair CHO^+ and $C_3H_3^+$, which is observed only in the case of 2-deoxy-D-ribose. This means that the $C_3H_3^+$ cation is ejected from such a moiety that involves one HCH at C(2) and two adjacent HOCH groups, i.e., the C(1,3) sites. In this dissociation channel, 2-deoxy-D-ribose must shake off all hydroxyl groups from the C(1,3) sites and a hydrogen atom from C(2).

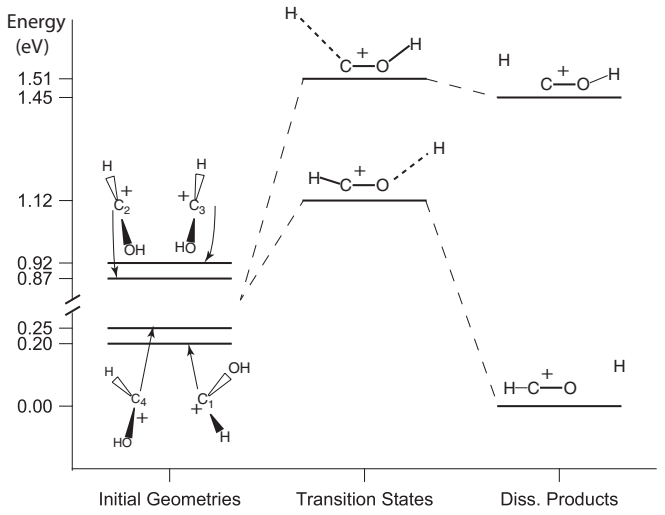

FIG. 10. Energy diagram describing different dissociation paths where hydrogen departs either HCO^+ or HOC^+. The sum of the total energies of the HCO^+ and H fragments is considered to be the zero point of the energy axis.

Patterns of ion pair (42,43) and possibly (43,43) in the DR, DRC, and DRD C 1*s* spectra (excluded here from the PEPIPICO maps) are indeed observed, but smear out badly, which makes analyzing them almost impossible. In contrast, the heaviest ion pair (43,43) corresponding to two $C_2H_3O^+$ ions is observed clearly only in the results of DRO C 1*s* measurements.

In summary, the HCOH-HCH moiety can produce $C_2H_3O^+$ (43) by losing a hydrogen from the hydroxyl group, and $C_2H_2O^+$ (42) by ejecting an additional hydrogen from the HCH group. Additionally, the HCOH-HCOH moieties are able to produce $C_2H_3O^+$ (43) by ejecting a hydroxyl group and also $C_2H_2O^+$ (42) by losing an additional hydrogen atom from another hydroxyl group, possibly in the form of H_2O (commonly known as water elimination). Lastly, the $C_3H_3^+$ (39) cation can be produced only from the C(1,2,3) sites in 2-deoxy-D-ribose by dissipating all hydroxyl groups [from C(1,3)] and also a hydrogen atom from the C(2) site.

8. Coincidences followed by O 1s core hole in 2-deoxy-D-ribose

In order to inspect site selectivity in photofragmentation of DRO, the sample was also studied at a photon energy of $h\upsilon = 578$ eV in the current experiment, recording the PEPIPICO patterns in coincidence with the O 1*s* photoelectrons. We have observed that the dissociation patterns from photofragmentation of DRO at the energy of $h\upsilon = 578$ eV are, within measurement error, the same as at the photon energy of $h\upsilon = 330$ eV, in coincidence with C 1*s* electrons. Hence, the dissociation process is not sensitive to the site of initial core ionization, likely because this information is largely lost in the Auger decay taking place prior to the dissociation.

D. Calculations

In this section, we will discuss why the amount of dissociation product CHO^+ (instead of CH_2O^+) dominates the PEPIPICO maps, and whether a hydrogen departs from O-H or C-H group in the dissociation channels discussed above. In this context, we inspect the normal vibrational modes of DR and the potential energy surface (PES) of the CH_2O^+ fragment in order to discover from which bond it is more energetically favorable for a migrating hydrogen to depart. The *ab initio* calculations were executed using unrestricted Hartree-Fock theory [22] at 6-311*pd* basis level [23] with the help of the GAMESS [24] software.

Single-point energies of $HCOH^+$ fragments with structures from different sites of D-ribose (see the Initial Geometries column in Fig. 10) were calculated as starting points for both transition states (TS) (see Fig. 10) where a hydrogen is about to depart from either bonding (HCO^+–H or H–COH^+). The minimum potential barrier [the energy difference of the single-point energy of $HCOH^+$ group at C(3) and the energy of the transition state HCO^+-H] for the O-H bond cleavage is 0.20 eV, and 0.59 eV for the C-H bond, suggesting that the hydrogen loss occurs predominantly from the former. These energy barriers are rather low and, at least for the O-H bond, can be easily overcome with vibrational excitations.

The vibrations of both sugar molecules and their energy-level populations were calculated to investigate the possible effect of the heating energy (92 °C or 365.15 K) on the vibrations. The average vibrational frequency of the stretching mode for the O-H bonds is (3743.96 cm^{-1}) 0.46 eV (very small variance of 0.00 eV), and the one for the C-H bonds is (2880.46 cm^{-1}) 0.36 eV, with negligible variance while D-ribose is in the ground state. The frequencies were scaled uniformly by a commonly used parameter of 0.9 to compensate for the overestimation of the used basis set. At the first O-H stretching vibrational energy level, the sugars should contain enough energy to overcome the O-H potential barrier, but the fact is that the measurement temperature is not high enough to enable the O-H stretching vibration; only vibration modes with lower wave numbers (e.g., those with wave number 300 cm^{-1}) are populated.

Generally speaking, the O-H bond would break more easily than the C-H bond in the fragmentation processes discussed in the current study. In addition, the first O-H stretching vibrational energy level should contain enough energy to overcome the O-H potential barrier, which would explain why the dissociating parent cations inherently produce CHO^+ cations rather than CH_2O^+ cations, as observed. However, the population of the first vibrational energy level is almost zero at the measurement temperature. Therefore, the main reason for the dissociating sugar molecules producing CHO^+ cations rather than CH_2O^+ cations is not clear.

IV. CONCLUSIONS

In this study, we have discovered that irradiating DNA and RNA sugars with soft x rays (here, 330 and 578 eV) will cause them to essentially explode into small fragments where the heaviest cationic fragment is 43 amu ($C_2H_3O^+$). The fragmentation mechanism induced by the core C 1*s* and O 1*s* level ionization of DNA sugar does not differ much from the one of RNA sugar. DNA sugar, with an additional HCH group compared to RNA sugar, enables the production of the [CH_3^+ (15), $C_2H_3^+$ (27)] and [CHO^+ (29), $C_3H_3^+$ (39)] ion pairs, which is not possible with RNA sugar. Otherwise, the characteristic

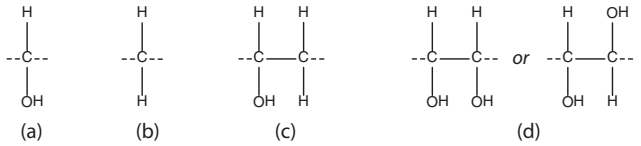

FIG. 11. Different moieties (as cation fragments) of the parent molecular ions involved in the different fragmentation pathways (see text).

dissociation channels of both sugars involve either a loss of a hydroxyl (-OH) group and/or a capture or a loss of H. In addition, bond cleavages in the dissociation processes involve any ring location in the pyranoses. In practice, this violent molecular explosion tends to strip the ring bonds of a molecule down to its fundamental building blocks, i.e., HCH and HCOH groups. However, as cation, the $HCOH^+$ radical or group is prone to eject a hydrogen atom in order to gain a more stable cationic form, HCO^+. Heavier cationic fragments, such as $C_2H_2O^+$ (42) and $C_2H_3O^+$ (43), formed by different combinations of the basic building blocks, are also rather common dissociation products.

According to the *ab initio* calculations performed, an O-H bonding has a higher tendency to eject hydrogen than a C-H bonding in the $CH_2O^+ \rightarrow CHO^+$ and H fragmentation process. Also, the O-H bond cleavage in $HCOH^+$ moieties is possible even at the first O-H stretching vibrational energy level, which would explain why the dissociation products are CHO^+s but not CH_2O^+s. However, the population of the first O-H stretching vibrational energy level at the measurement temperature (92 °C or 365.15 K) is minimal, and the thermal energy is, therefore, expected to be distributed to other vibrational modes which have much smaller wave numbers. Thus, the main reason for the dissociating sugar molecules producing CHO^+ cations rather than CH_2O^+ cations is not clear.

In general, the fragmentation patterns of D-ribose and 2-deoxy-D-ribose can be summarized to involve the following general steps (see Fig. 11):

(i) The HCOH group [see Fig. 11(a)] serves as a precursor moiety creating aldehyde cations by dissipating a hydrogen from the hydroxyl group, or capturing a hydrogen atom from a neighboring group during the fragmentation process, to yield CH_3O+.

(ii) The HCH (14) moiety [see Fig. 11(b)] has a tendency to separate intact and it can also capture a hydrogen from a neighboring HCOH moiety resulting in CH_3^+ (15).

(iii) The moiety shown in Fig. 11(c) can produce $C_2H_3O^+$ (43) by losing a hydrogen from the hydroxyl group, and $C_2H_2O^+$ (42) by ejecting an additional hydrogen from the HCH group. Furthermore, the same moiety can produce $C_2H_3^+$ (27) by ejecting a whole hydroxyl group, and $C_2H_4^+$ (28) by recapturing the hydrogen atom from the eliminated hydroxyl group.

(iv) The moieties shown in Fig. 11(d) are capable of producing $C_2H_3O^+$ (43), by ejecting a hydroxyl radical, and $C_2H_2O^+$ (42), by losing a hydroxyl group and a hydrogen atom from another hydroxyl group, possibly in the form of H_2O (commonly known as water elimination).

With the dissociation mechanisms described above, one can expect the consequences of soft-x-ray irradiation to be lethal to the DNA and RNA helix, especially considering the fragments departing from the carbon C(3) and C(5) sites, which are connected to the phosphate backbone in the DNA and RNA chain. It is possible that the cations of the dissociated sugar stay bonded with adjacent phosphates and, therefore, due to their nonthermal kinetic energy, attempt to pull the phosphates or parts of the phosphates out of their locations, causing additional damage to the helix. More likely, however, the cationic fragments thrust out from their location tearing also the bonds of the adjacent phosphates, and may collide with other adjacent parts of the DNA and RNA helix, creating damage clusters. Either way, soft-x-ray damage is likely to lead to multiple and clustered strand breaks in the DNA and RNA helix. This might be valid for DNA and RNA helices clustered in a small area (thus minimizing the space between parts of the helices). However, moieties in DNA and RNA helices far from the Coulomb explosion points are well protected (by water molecules filling the space in biological environments) from the cationic fragments, according to Liu *et al*. [25].

ACKNOWLEDGMENTS

Financial support from the Academy of Finland, the Turku University Foundation, the EU Transnational Access to Research Infrastructures programme, and the Graduate School of Materials Research of the Ministry of Education of Finland is acknowledged. M.A.H. acknowledges funding from the Natural Science and Engineering Research Council of Canada and the Canadian Space Agency. The authors thank the staff of MAX-lab for their help during the experiments.

[1] L. P. Guler, Y.-Q. Yu, and H. I. Kenttämaa, J. Phys. Chem. A **106**, 6754 (2002).

[2] C. von Sonntag, *The Chemical Basis of Radiation Biology* (Taylor & Francis, London, 1987), p. 116.

[3] S. Ptasinska, S. Denifl, P. Scheier, and T. D. Märk, J. Chem. Phys. **120**, 8505 (2004).

[4] G. Vall-llosera, M. A. Huels, M. Coreno, A. Kivimäki, K. Jakubowska, M. Stankiewicz, and E. Rachlew, Chem. Phys. Phys. Chem. **9**, 1020 (2008).

[5] K. Fujii, K. Akamatsu, and A. Yokoya, Surf. Sci. **528**, 249 (2003).

[6] Z. Deng, I. Bald, E. Illenberger, and M. A. Huels, Phys. Rev. Lett. **95**, 153201 (2005).

[7] C. J. Danby and J. H. D. Eland, Int. J. Mass Spectrom. **8**, 153 (1972).

[8] M. Simon, T. LeBrun, P. Morin, M. Lavollée, and J. L. Maréchal, Nucl. Instrum. Methods B **62**, 167 (1991).

[9] M. Simon, P. Morin, P. Lablanquie, M. LavollCe, K. Ueda, and N. Kosugi, Chem. Phys. Lett. **238**, 42 (1995).

[10] T. A. Field and J. H. D. Eland, Meas. Sci. Technol. **9**, 922 (1998).

[11] C. Harada, S. Tada, K. Yamamoto, Y. Senba, H. Yoshida, A. Hiraya, S. Wada, K. Tanaka, and K. Tabayashi, Radiat. Phys. Chem. **75**, 2085 (2006).
[12] E. Kukk, R. Sankari, M. Huttula, A. Sankari, H. Aksela, and S. Aksela, J. Electron Spectrosc. Relat. Phenom. **155**, 141 (2007).
[13] E. Itälä, E. Kukk, D. T. Ha, S. Granroth, A. Calö, L. Partanen, H. Aksela, and S. Aksela, J. Chem. Phys. **131**, 114314 (2009).
[14] E. Itälä, D. T. Ha, K. Kooser, E. Rachlew, M. A. Huels, and E. Kukk, J. Chem. Phys. **133**, 154316 (2010).
[15] M. Huttula, S. Heinäsmäki, H. Aksela, E. Kukk, and S. Aksela, J. Electron Spectrosc. Relat. Phenom. **156-158**, 270 (2007).
[16] E. Kukk, computer code Spectral Analysis by Curve Fitting (SPANCF)[http://www.physics.utu.fi/en/research/material_science/Fitting.html, 2009].
[17] M. Bässler, A. Ausmees, M. Jurvansuu, R. Feifel, J.-O. Forsell, P. de Tarso Fonseca, A. Kivimäki, S. Sundin, S. L. Sorensen, R. Nyholm, O. Björneholm, S. Aksela, and S. Svensson, Nucl. Instrum. Methods Phys. Res. A **469**, 382 (2001).
[18] J. H. D. Eland, Laser Chem. **11**, 259 (1991).
[19] A. C. O. Guerra, D. J. S. Flora, R. D. L. Santos, G. B. Ferreira, and C. C. Turci, Rev. Bras. Aplic. Vac. (Braz. J. Vac. Applic) **27**, 85 (2008).
[20] F. Alvarado, J. Bernard, B. Li, R. Brédy, L. Chen, R. Hoekstra, S. Martin, and T. Schlathölter, Chem. Phys. Chem. **9**, 1254 (2008).
[21] E. Itälä, D. T. Ha, K. Kooser, E. Nõmmiste, U. Joost, E. Kukk, Int. J. Mass Spectrom. **306**, 82 (2011).
[22] J. A. Pople and R. K. Nesbet, J. Chem. Phys. **22**, 571 (1954).
[23] R. Krishnan, J. S. Binkley, R. Seeger, and J. A. Pople, J. Chem. Phys. **72**, 650 (1980).
[24] M. W. Schmidt, K. K. Baldridge, J. A. Boatz, S. T. Elbert, M. S. Gordon, J. H. Jensen, S. Koseki, N. Matsunaga, K. A. Nguyen, S. Su, T. L. Windus, M. Dupuis, and J. A. Montgomery, J. Comput. Chem. **14**, 1347 (1993); M. Gordon, computer code GAMESS, [http://www.msg.chem.iastate.edu/gamess/].
[25] B. Liu, S. B. Nielsen, P. Hvelplund, H. Zettergren, H. Cederquist, B. Manil, and B. A. Huber, Phys. Rev. Lett. **97**, 133401 (2006).